1.6 Some aspects of numerical modelling for additive manufacturing

Stéphane Gounand, Olivier Asserin, Anaïs Baumard, Séverine Paillard

Some aspects of numerical modelling for additive manufacturing

GOUNAND, Stéphane
BAUMARD, Anaïs
ASSERIN, Olivier
PAILLARD, Séverine

Goal: not an exhaustive review (very good one exist (DebRoy...) but subjectively chosen aspects that seem important to us.

1. Introduction

Super-insulating architectural materials based on ceramics or ultra-light and resistant hierarchical amorphous structures, shapes that is impossible to manufacture by conventional machining, such as minimal periodic surfaces like gyroids or open-pore organised metallic foams to maximise the solar illumination received for Thermodynamic Solar Power Plants. They are also "cold" fuel pellets to gain margins in case of loss of primary coolant, new Cobalt-free composition gradient hard coatings based on Nickel to replace Stellite, or a no longer manufactured EDF manual valve control, a monobloc grid for holding fuel needles that cannot be made by conventional machining, a rotor lightened by means of lattices, tissues for organ reconstruction or for therapeutic issues.
These are also super materials that can withstand severe environmental constraints thanks to a combination of properties or antagonistic functions such as hardness-ductility that would have been impossible to obtain with a single material. But also components that can no longer be produced or concepts that cannot be realised with conventional processes.

Achieving parts with the expected characteristics and target properties requires high manufacturing quality in a reproducible and cost-efficient manner. This can be achieved by improving productivity, reducing the high cost of raw materials, and increasing the products and manufacturing processes performance.

First Need, to control the manufacturing process. Additive manufacturing has already demonstrated the ability to produce conform parts comparable with their conventionally processed. However, the poor repeatability, reproducibility, of the machines is an obstacle. Users would like to make progress in understanding the influence of operating parameters and raw material properties in order to control manufacturing, tailor the properties and functions, and create architectural structures.

Second Need, to ensure the quality and performance of the product. Product performance requires a better scientific understanding of additive manufacturing processes, including the influence of microstructure on properties and ultimately on the service life of manufactured parts. It is necessary to understand the effect of composition on microstructure and properties under complex thermal cycles.
Process simulation could help in this regard. However, taking all physical phenomena into account requires modelling at different scales, this development will take place

over time and requires input data that are not easy to measure and experimental validation.

2. Overview of modelling approaches for additive manufacturing

2.1 Why model and simulate ?

The reduction in the number of components, facilitated functional integration, concatenation of functions, material savings, production as close as possible to the sites, the offer of alternative solutions to certain current sources of supply, and rapid prototyping, all lead to easier manufacturing and control, reduced lead times and costs, improved responsiveness and overall performance and productivity.
However, additive manufacturing ultimately concerns relatively few components. These will be high value-added parts subject to very specific or multiple constraints, or components that can no longer be produced or concepts that are not possible with conventional processes. It is mainly the improvement of performance that is expected, and it is then the cost/performance ratio that establishes the interest of additive manufacturing for the components.

Improving performance concern the product with antagonistic functional properties challenging the Ashby diagrams and feeting severe constrains, and also the manufacturing process by simplifying assembly, the achievement of daunting concepts with conventional processes.

One of the main obstacles to commercial and industrial use of additive manufacturing are the low level of repeatability of the manufacturing process and reproducibility between machines. In order to improve performance, the entire manufacturing process chain must be under control, from the raw material through the process to the finishing treatments. Thus, it is important to understand the effect of the many parameters that come into play at each stage. For example, the effect of the trajectory and speed of the deposits on the morphology of the beads, on the thermal cycles. We would also like to be able to explain the lack of fusion, the instabilities of the bath, the cracking. Particularly, in SLM, there are also problems of denudation, balling, gas distribution which will have an influence on defects such as porosities, and the control of deformations and stresses, the magnitude of which can lead to the rupture of supports or to important deformations forcing multiple construction stops and scrapping.

2.2 Modelling approaches, Multiscale and multiphysics aspects

The additive manufacturing process consists of creating objects by a sequence of successive layers of material. The material can be deposited by extrusion (FDM) for polymers, ceramic pastes, or in the form of molten metal drops brought by wire or by a fusible electrode, or sprayed powder (DMD), for thermoplastics or metal alloys. The material may also be already present and then selectively consolidated (coalesced and then solidified or polymerized) by an additional heating source such as a laser or electron beam as in the case of powder bed, or a liquid polymer resin.

For metal fabrication processes with powder or wire such as SLM, DMD, WAAM, WLAM three scales can be distinguished. That of the powder particles which are considered discrete or the so-called microscopic wire, that of the weld-pool or powder bed according to the so-called mesoscopic manufacturing process where the powder is considered continuous and that of the so-called macroscopic part where the material is considered homogeneous. Each of these scales requires special modelling. At the microscopic scale, it is the coating of the powder, the interaction of the material process on the powder grains, the phenomena of denudation, sintering, the shape of the molten zone, the evaluation of the absorption and diffusion of energy that are of interest. At the mesoscopic scale the material process interaction is considered in the molten pool, but the material is considered continuous. Molten pool dynamics, deposit shape, microstructure, dilution, defects such as porosities, hot cracking, bath instabilities, models of phase transformations, convection, radiation, evaporation, conduction, absorption, reflection, of gravity, magnetohydrodynamics, coalescence, capillarity, wetting, solidification shrinkage are used with various methods such as Lattice Boltzmann (LB), Discrete Element Method (DEM), Smoothed-particle hydrodynamics (SPH), Volume Of Fluid (VOF) and Finite Elements (EF).
In DMD, the powder jet in the nozzle is modelled as well as the laser material interaction at the nozzle exit on the jet and on the workpiece, followed by the material input and the dynamics of the pool.
With wire, the material process interaction is modeled at the wire and part scale, then the material input is sometimes modeled at the drop scale. When the process is an electric arc, electromagnetism is added for the pool dynamics and the arc plasma, the model then becomes magnetohydrodynamics.
At the macroscopic scale, models are based on thermomechanics and thermometallurgy. The treatment is quite similar between material deposition and powder bed processes. In particular, the energy transfer to the workpiece is either the result of microscopic-mesoscopic calculation, or imposed in the form of an equivalent heat source calibrated on previous experiments.
At the mesoscopic and macroscopic scales, solidification, microstructural transformations, residual stresses and deformations are also considered. However, the mesoscopic scale commonly concerns not more than one bead. Thus, changes in these quantities over time and under the effect of other deposits are not taken into account at this scale.
A comprehensive review of all the components and methods of additive manufacturing modelling could be found in Panagiotis Stavropoulos "Modelling of additive manufacturing processes: a review and classification" in Manufacturing Rev. 5, 2 (2018) https://doi.org/10.1051/mfreview/2017014
All of these models have not been established recently, one can find all the DNA of welding simulation with the specificity of the very large number of passes, sometimes very thin beads and stronger thermal gradients (SLM). The developments already made in welding are already a good basis, nevertheless the very large number of passes calls for important numerical challenges to overcome and the very strong thermal gradients require new models and validation experiments.
For powders, morphology (sphericity, size distribution), chemistry will have a decisive impact, as will wires in WLAM, WAAM. Taking these into account requires microscopic and mesoscopic modelling. The implementation of the discrete element

method and thermokinetic modelling as Calphad http://www.calphad.org/ by the tools of thermodynamic calculations (Thermo-Calc, OpenCalphad http://www.opencalphad.org/) and diffusion (DICTRA (module of Thermo-Calcl).
In addition, the manufacturing machines have many operating parameters whose adjustment is complex by the difficulty to be under repeatability and reproducibility conditions. The user wishes to be able to predict the morphology of the cord and to have an operative control. Experimental designs (screening) combined with simple simulations would make it possible to identify trends.

3. Focus 1: multiphysics of liquid metal pool

Main contributor: Stéphane Gounand
In this section, we discuss some aspects of the physical and numerical modelling of liquid metal pools that arise during welding or additive manufacturing processes. Indeed, despite its quite small dimensions compared to the workpiece, the liquide metal pool has an important role in determining the local distribution of temperature. This is due to the fact that intense convective phenomena generally occur in the molten metal.
In section 3.1, we describe the physical setting of liquid metal pool modelling, first in the context of welding and then in the context of additive manufacturing. This leads us to consider in section 3.2 the effects of one of the main driving force which act in the melt pool which is surface tension. From a numerical viewpoint, the small size of the weld pool relative to the workpiece leads to stringent constraints on the mesh, an aspect we discuss in section 3.3.
Notice that the computation and meshes of this section were obtained with our in-house Finite Element toolbox Cast3M[1].

3.1 Physical Context

Before going on to Additive Manufacturing (AM), as an example of complex multiphysics model, we describe what physically happens near the heat source in the case of the industrial-grade Tungsten Inert Gas (TIG) welding process.

3.1.1 Example of Tungsten Insert Gas (TIG) welding

TIG welding process

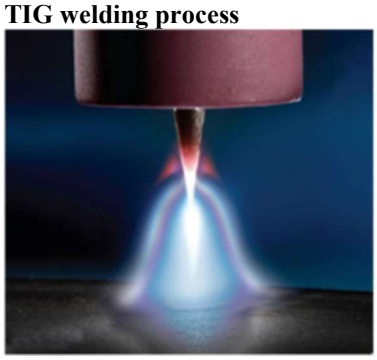

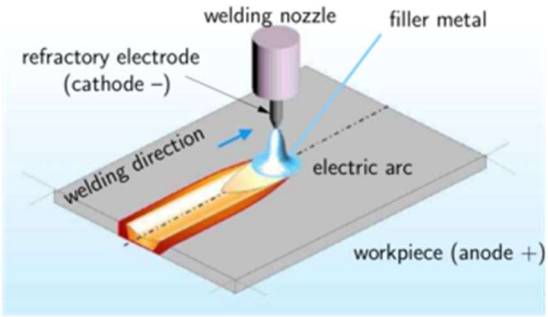

figure
Tungsten Inert Gas (TIG) welding process: arc (left) and schematic diagram (right) [2]
[fig:tig]

The TIG metal assembly process uses a Tungsten, refractory electrode, an inert gas (Argon in general) brought through a nozzle which acts both as a plasmagenous medium and as a barrier against oxidation, and a generator to trigger the plasma. This plasma acts as the heat source for melting both the base metal and a filler wire (figure 1).

Multiphysical aspects of TIG welding

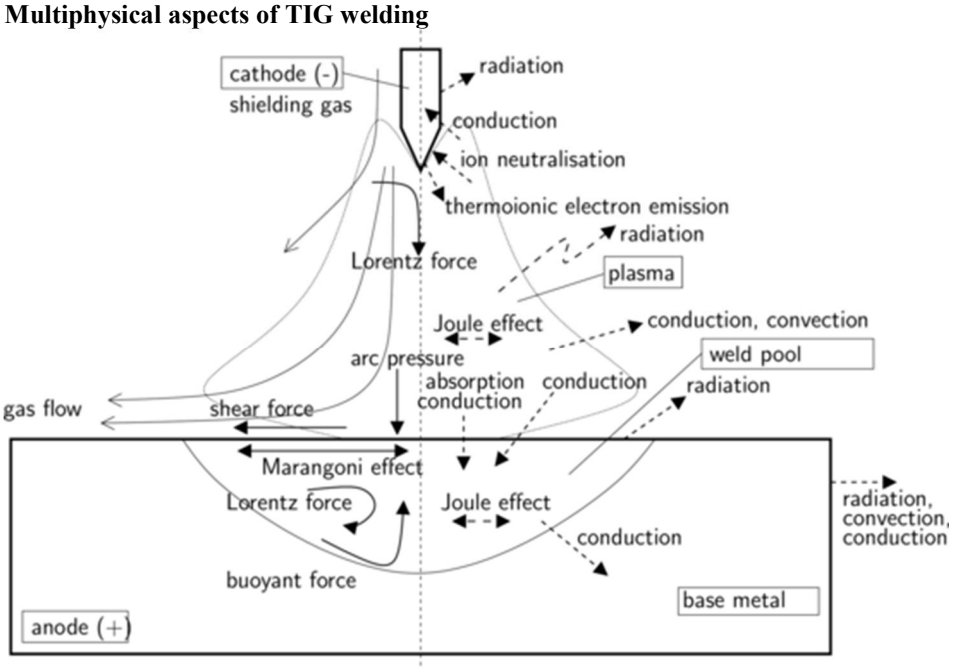

Physical phenomena in TIG process [3].

A close-up view on the physical phenomena taking place in the plasma and in the base metal gives the daunting diagram 2 which isn't nearly exhaustive: for instance the plasma-weld pool interface deforms and metal evaporation can occur, the weld pool-base metal interface is subject to all the complexity of metal solidification…Thermally important is the fact that both the arc plasma and the weld pool do not remain static and flow quite rapidly: $\approx 300\mathrm{m.s^{-1}}$ in the plasma and $0.1\mathrm{m.s^{-1}}$ in the melt pool. In general, the main driving force for the flow is the electromagnetic Lorentz force in the arc and the Marangoni force (due to surface tension) in the weld pool.

3.1.2 From welding to additive manufacturing

Going from welding to additive manufacturing processes, we generally have that very similar physical phenomena occur. For example, the TIG-WAAM (Wire Arc Additive Manufacturing) process and TIG are physically similar. However, going from assembly to manufacturing entails some differences, mainly: metallic powder related aspects and geometry related aspects. In welding processes, the local metal-heat source geometry roughly looks like a plate while for AM (except at the beginning), it will rather look like

a fin, which leads to different thermal pumping behavior. Also of importance are the differences in characteristic scales in the process parameters as shown in table:

Typical characteristic scales

Parameter	Welding (TIG)	Additive manufacturing (SLM)
$P_{\text{heat source}}$	1000 W	100 W
$r_{\text{heat source}}$	5.e-3 m	5.e-5 m
$\mathbf{u}_{\text{heat source}}$	1.e-3 m.s^{-1}	1. m.s^{-1}
Metal Addition	Filler wire	Powder

Typically, AM will use faster, more intense heat sources with a smaller length scale compared to welding. This smaller length scale notably implies: on the physical side, higher temperature gradients and surface tension effects and on the numerical side, meshing difficulties. We briefly elaborate on these two aspects in subsection 3.2 and 3.3.

3.2 Surface tension phenomena

We first discuss the physics of surface tension forces before describing its effects on a melt pool.

3.2.1 Surface tension forces in 2D

Normal (left) and tangential (right) surface tension forces

To get a quick grasp on how surface tension works, it is easier to picture it in 2D in a discrete setting and remember the variational interpretation of surface tension: a force that tries to minimize a γ-weighted surface energy ($\int_S \gamma \, \mathrm{d}S$). $\gamma$is the surface tension in N.m^{-1}.

Normal component First we consider figure 3 (left) which represents a bent surface of two segments of same γ. The force acting on the end node of a segment is directed inward and tangentially trying to shrink the segment with magnitude γ(a 2D force has unit N.m^{-1}). The net force exerted by the two segments on the middle node is thus obtained by the parallelogram of force shown on the figure. It is directed in the normal direction (in an averaged sense) to the surface with a norm that grows with the variation of slope between the two segments (a discrete curvature). Going back to the continuous setting, it can be shown that following formula for the surface tension force holds: $\mathbf{f_n} = \frac{\gamma}{R}\mathbf{n}$ where $\frac{1}{R}$ is the curvature.

Tangential component Second we consider figure 3 (right) which represents an unbent surface of two segments with different γ (higher for the left segment). Now, the net force exerted by the two segments on the middle node is directed in the tangential direction to the surface towards higher γ with a norm that grows with the variation of γ between the two segments (a discrete gradient). Going back to the continuous setting, it can be shown that following formula for the surface tension force on a flat surface with varying γ holds: $\mathbf{f_t} = \nabla_s \gamma$ where ∇_s is the surface gradient.

Surface tension force Now, adding the normal $\mathbf{f_n}$ and tangential $\mathbf{f_t}$ components, we get the whole surface tension force $\mathbf{f}_{\text{Tension}} = \frac{\gamma}{R}\mathbf{n} + \nabla_s\gamma$. The normal component is the **geometric** part, while the tangential component is the **Marangoni** part of the surface tension force and acts as a **shearing** force.

3.2.2 Liquid metal pool, Marangoni effect

In the case of liquid metal pool, we generally consider that the Marangoni effect is mainly due to the variation of γ with temperature T. Indeed, γ is also sensitive to the concentration of so-called tensioactive elements (sulfur S concentration is frequently considered for stainless steel materials) but this concentration can be assumed constant in the weld pool due to convective mixing. We then write: $\nabla_s\gamma = \mathrm{d}\gamma/\mathrm{d}T \times \nabla_s T$ with $\mathrm{d}\gamma/\mathrm{d}T$ the temperature derivative of surface tension and $\nabla_s T$ the surface temperature gradient.

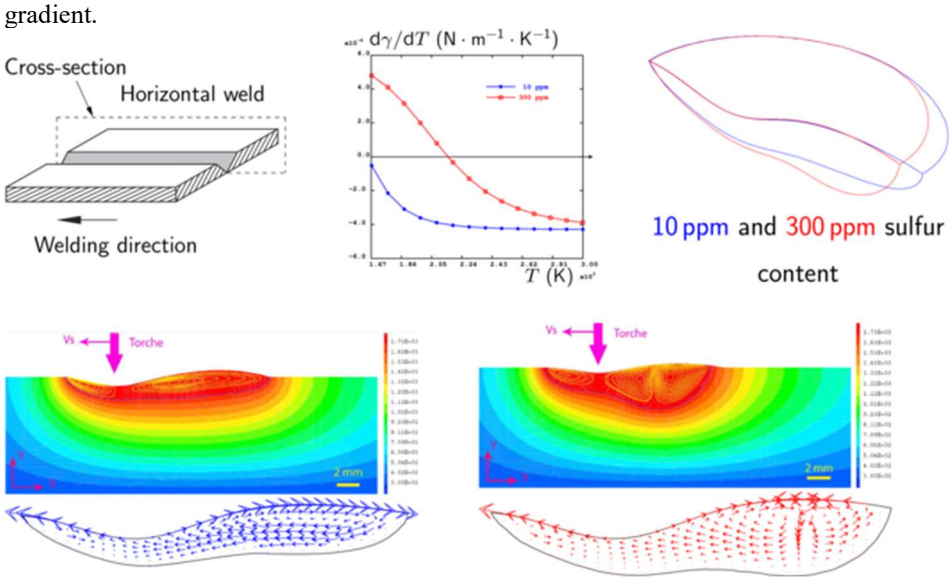

Melt pool shapes [4]

Now, $\mathrm{d}\gamma/\mathrm{d}T$ is not constant. Figure 4 (middle, up) shows the temperature dependency of $\mathrm{d}\gamma/\mathrm{d}T$ for two sulfur concentration (10 ppm blue and 300 ppm red) for 316L stainless steel. Notice that $\mathrm{d}\gamma/\mathrm{d}T$ even changes sign for the 300ppm case. This leads to quite different flows in the melt pool together with different melt pool shapes (figure 4) for the 10ppm and 300ppm cases.

The melt pool shapes are obtained for the case of welding in flat position. In AM, it is expected that the melt pool will be smaller but with more intense surface tension effects: higher temperature gradients calls for higher Marangoni flow (velocities of $\approx 10\mathrm{m.s^{-1}}$ have been reported) and interface rounding geometric effect. Also, we didn't discuss the wetting boundary conditions (triple line between melt pool, base metal and gas) but its importance could be paramount in the case of AM.

3.3 Meshing

For a numerical computation of a melt pool to be meaningful, sufficient meshing of the melted part should achieved. This a problem in Additive Manufacturing because the melt pool is quite small relative to the manufactured workpiece.

3.3.1 Manual meshing

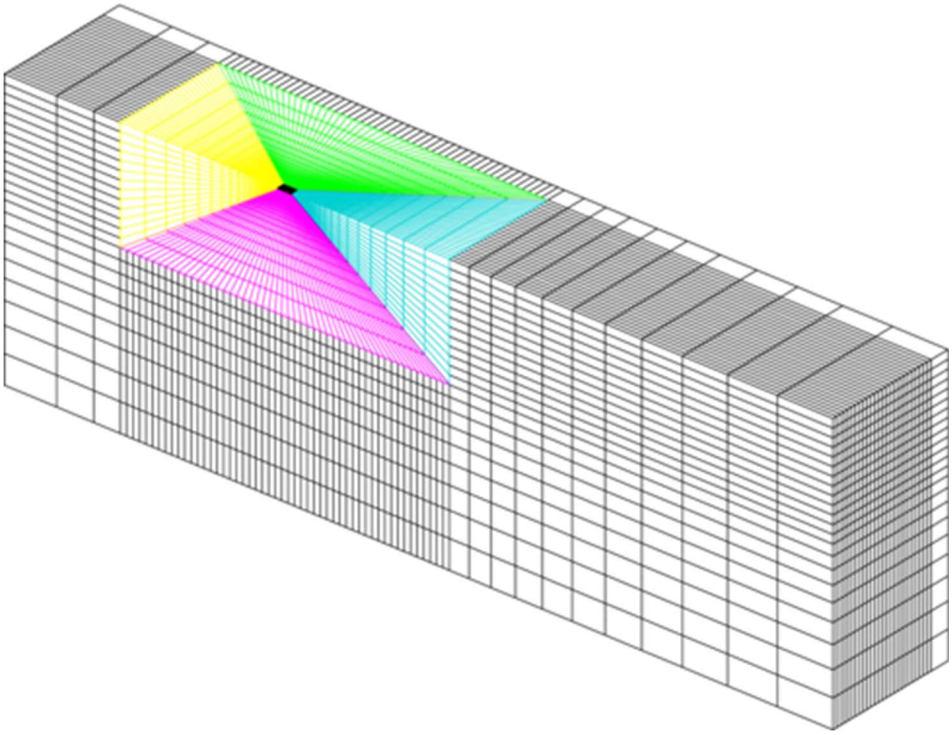

Manually tailored mesh

For a typical melt run on a simple plate geometry with the process parameters of the additive manufacturing case of section 4, we can come up with the manually tailored mesh of figure 5. Notice that the melt pool is barely visible at the intersection of the four coloured derefinement parts of the mesh. It is clear that manual meshing of more complex and time-evolving geometries can be very difficult.

3.3.2 Automatic meshing

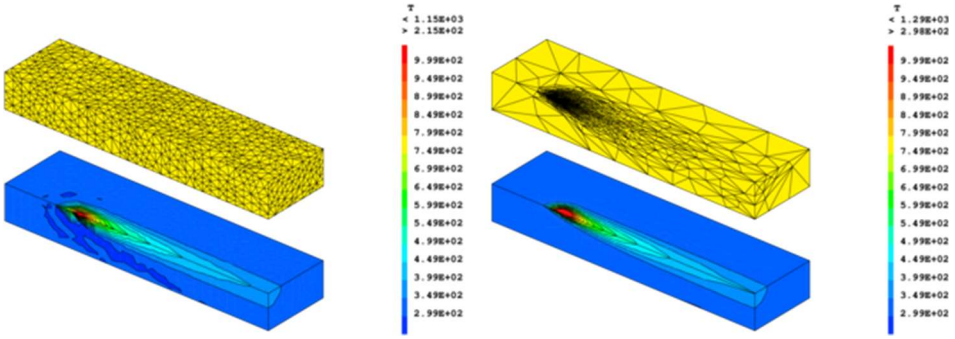

Automatically adapted mesh

In order to circumvent the difficulty of manual meshing, one could rely on automatic meshing. In figure 6, we present some preliminary numerical experiments of the use of anisotropic adaptive meshing for a simplified melt run test case (only thermal effects are modelled with no melt pool modelling). Figure 6 (left) shows the initial non-adapted regular mesh and the corresponding numerical solution for the temperature field. This field shows numerical oscillations (dark blue color) due to unsufficient mesh refinment. Figure 6 (right) shows the anisotropic adapted mesh that was optimised iteratively from the initial mesh and solution. The temperature field is now correctly resolved and free from numerical oscillations with the same number of mesh nodes.

Notice that we have focused on conforming meshing strategies (no hanging nodes) but non-conforming meshing are possible. Also, other numerical components are frequently needed to complement the meshing strategy: projection from one mesh to another, error estimators to drive the mesh adaptation process, modification of the numerical method to account for non-conforming meshes…

4. Focus 2: Numerical prediction of grain structures formation in additively manufactured 316L stainless steel

Main contributor: Anaïs Baumard

In this section, we discuss a numerical method for predicting grain structures formation during Laser Beam Melting of single track 316L Stainless Steel [5].

4.1 Context

Additive Manufacturing processes offer the possibility to reduce manufacturing time and material waste, and allows for the creation of structures with complex design. However, an anisotropic mechanical behaviour is frequently observed in components manufactured by AM processes. This anisotropy is directly linked to the component's grain structure characteristics, which are dependant on the process parameters. For this reason, the formation of grain structure during Laser Beam Melting (LBM) of a 316L stainless steel is investigated in this paper.

For that purpose, an approach combining experiments and numerical simulations is adopted. In section 4.2, the experimental setup is described. In section 4.3, the numerical modelling approach follows with a comparison of grain characteristics obtained experimentally and numerically (section 4.4).

4.2 Experimental setup

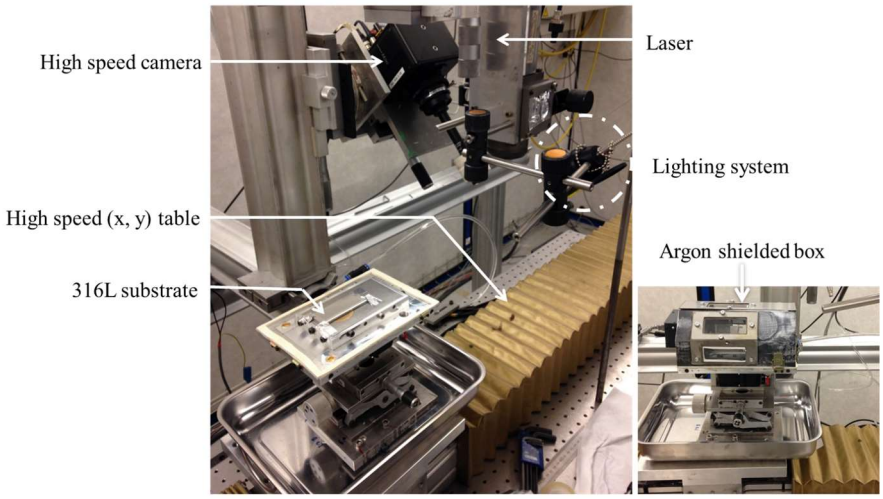

Powder bed laser fusion installation (PIMM – ENSAM, France)

Powder bed laser installation (PIMM-ENSAM, France)
The experimental part consists in building instrumented one-layer 316L single-tracks by LBM. The study of the single-tracks allows for the characterization of the grains (microstructural analysis is carried out by optical microscopy and Electron Backscatter Diffraction), and the optical instrumentation allows for the observation of the molten pool. The one layer single-track geometry has been chosen in order to limit the building parameters involved in fabrication. Indeed, by choosing a single-track geometry, hatching distance and scanning strategy do not influence the built part. Moreover, as it is a first model validation work, the presented results are limited to melt-runs, which are equivalent to single-tracks but without powder. The process parameters are: laser power (P) of 400 W with a focal spot size of 150 µm, a wavelength of 1030 nm and a velocity (v) of 400 mm.s^{-1}. An airtight box filled with argon is used in order to reduce oxygen content (less than 100 ppm).

4.3 Numerical modelling

The numerical modelling is based on a three-dimensional “CAFE” model, which couples Cellular Automata (CA) and Finite Elements (FE) simulations. It is used to predict grain formation during the LBM process.

4.3.1 Thermal analysis

The first part of the model consists in doing the thermal analysis which consists in solving the heat equation in 3D with a Finite Element method.

$$\rho C_p \frac{\partial T}{\partial t} = \Delta T + q$$

The calculations are carried out with the Cast3M software [1]. The input parameter for this equation (q) is a modelled volumetric heat source that accounts for both the true heat source (laser) and the convective effects in the molten pool. We choose a Goldak (double-ellipsoïd) volumetric heat source that has 4 geometric parameters (half-width, penetration, front and rear half-length of each ellipsoid) and 2 physical parameters (power and velocity). The physical parameters are identical to the laser's. The geometric parameters are chosen so as to approximately fit the experimentally observed molten pool boundary geometry (width, depth and length).

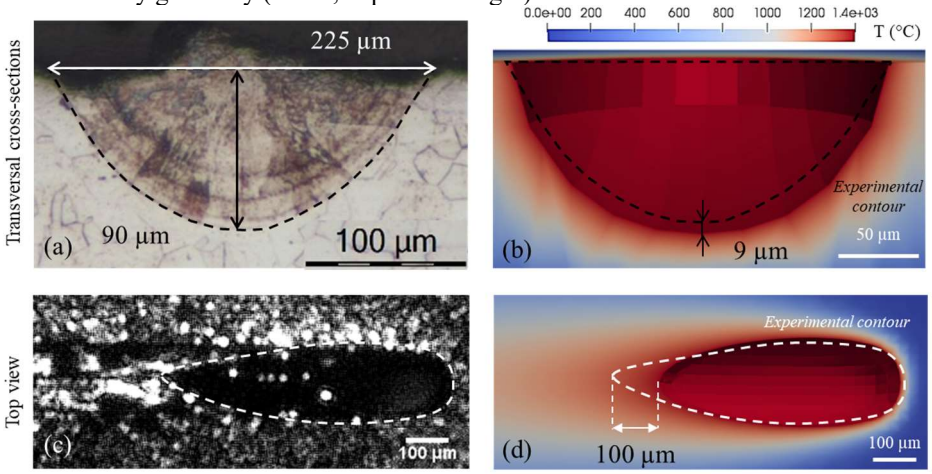

Comparisons of experimental, (a) and (c), and numerical, (b) and (d), dimensions of the molten pool observed in melt-runs

Figure 8 shows a good agreement between the dimensions of the experimental and numerical molten pool dimensions, validating the use of a Goldak source. Notice that the geometric parameters of the Goldak heat source change whenever a process parameter changes. For example, the geometric parameters are not the same for single tracks and melt runs.

4.3.2 Solidification growth modelling

The grain growth model is based on the cellular automaton (CA) model defined by Gandin and Rappaz [6], which we do not detail here. It focuses on grain structure evolution during solidification accounting for two main physical phenomena, namely nucleation and grain growth. The input data for the CA model are the temperatures calculated in the FE model. Notice that we only have a weak coupling between these two models because we assume that the solidification calculations have no influence onto the thermal ones. Also, the cellular automaton mesh is a cartesian grid which is much finer than the FE mesh: interpolation is used to obtain the CA temperature from

the FE computations. The time steps may also be different: they are generally smaller for the CA which is an explicit numerical method.

4.4 Experimental-numerical comparison

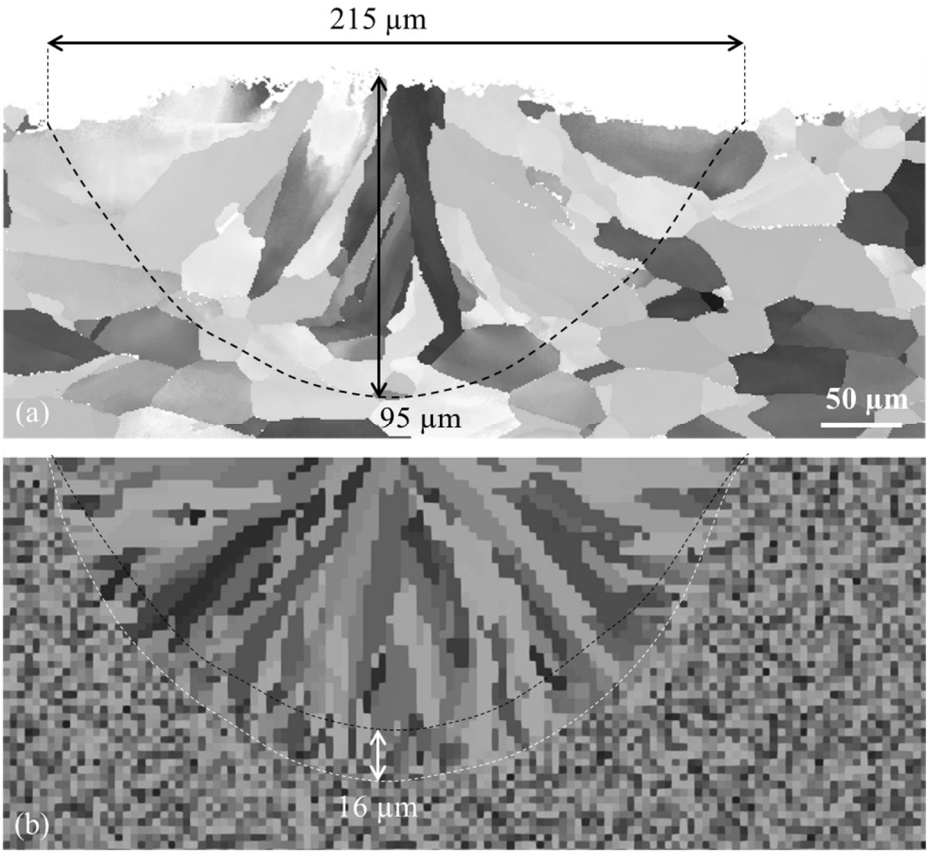

(a) Experimental and (b) numerical transversal cross-sections of grain structure obtained for melt-runs

Eventually, numerical grain characteristics resulting from the simulations are compared to the experimental ones in figure 9 on transversal cross-sections. Both experimental and numerical images show visible columnar grains, with perpendicular orientation with respect to the solid interface. The morphology and width of the molten pool are almost identical, but numerical pool's depth is slightly longer. Also, it is clearly visible that the grain are thinner and more numerous in the numerical results. It is assumed that this is because the grain structure of the substrate is not correctly modelled. Indeed, in this current algorithm the substrate is composed of as many grains as cells, and each cell has a specific crystallographic orientation. Regardless, these numerical results are promising.

Future prospects for this study are numerous. Numerically, better modelling of the substrate's grain structure, multi-track configuration with thermal cycling or even

multiphysics modeling of the laser and molten pool come to mind. Experimentally, further analysis of grain structure (not only in transversal cross-sections) varying the process parameters would be interesting, keeping in mind the combined numerical experimental approach.

[1] “Cast3m Web site.” http://www-cast3m.cea.fr/, 2020.
[2] M.-C. Nguyen, “Modélisation et simulation multiphysique du bain de fusion en soudage à l’arc TIG,” PhD thesis, Université d’Aix-Marseille I, 2015.
[3] M. Brochard, “Modèle couplé cathode-plasma-pièce en vue de la simulation du procédé de soudage à l’arc tig,” PhD thesis, Université de Provence (Aix-Marseille I), 2009.
[4] M. C. Nguyen, M. Medale, O. Asserin, S. Gounand, and P. Gilles, “Sensivity to welding positions in GTA welding with a 3D multiphysics numerical model,” *Numerical Heat Transfer, Part A: Applications*, vol. 71, no. 3, pp. 233–249, 2017.
[5] A. Baumard, D. Ayrault, O. Fandeur, C. Bordreuil, F. Deschaux-Beaume, and A.-L. Vetele, “Numerical prediction of grain structures formation during Laser Beam Melting of Single-Track 316L Stainless Steel,” *Computational Materials Science*, 2020.
[6] C.-A. Gandin and M. Rappaz, “A coupled finite element-cellular automaton model for the prediction of dendritic grain structures in solidification processes,” *Acta Metallurgica Materialia*, vol. 42, no. 7, pp. 2233–2246.